8-1-2008

Gate-induced quantum-confinement transition of a single dopant atom in a silicon FinFET

G P. Lansbergen
Delft Univ Technol, Kavli Inst Nanosci

R Rahman
Purdue University

C J. Wellard
Univ Melbourne

I Woo
Purdue University

J Caro
Delft Univ Technol, Kavli Inst Nanosci

See next page for additional authors

Gate-induced quantum-confinement transition of a single dopant atom in a silicon FinFET

G. P. LANSBERGEN[1]*, R. RAHMAN[2], C. J. WELLARD[3], I. WOO[2], J. CARO[1], N. COLLAERT[4], S. BIESEMANS[4], G. KLIMECK[2,5], L. C. L. HOLLENBERG[3] AND S. ROGGE[1]

[1]Kavli Institute of Nanoscience, Delft University of Technology, Lorentzweg 1, 2628 CJ Delft, The Netherlands
[2]Network for Computational Nanotechnology, Purdue University, West Lafayette, Indiana 47907, USA
[3]Center for Quantum Computer Technology, School of Physics, University of Melbourne, VIC 3010, Australia
[4]InterUniversity Microelectronics Center (IMEC), Kapeldreef 75, 3001 Leuven, Belgium
[5]Jet Propulsion Laboratory, California Institute of Technology, Pasadena, California 91109, USA
*e-mail: G.P.Lansbergen@tudelft.nl

Published online: 15 June 2008; doi:10.1038/nphys994

The ability to build structures with atomic precision is one of the defining features of nanotechnology. Achieving true atomic-level functionality, however, requires the ability to control the wavefunctions of individual atoms. Here, we investigate an approach that could enable just that. By collecting and analysing transport spectra of a single donor atom in the channel of a silicon FinFET, we present experimental evidence for the emergence of a new type of hybrid molecule system. Our experiments and simulations suggest that the transistor's gate potential can be used to control the degree of hybridization of a single electron donor state between the nuclear potential of its donor atom and a nearby quantum well. Moreover, our theoretical analysis enables us to determine the species of donor (arsenic) implanted into each device as well as the degree of confinement imposed by the gate.

Dopants have a longstanding and vital role in semiconductor technology as passive charge providers. In the past decade, they have been the subject of renewed interest for their potential use as the basic elements in Si quantum electronics[1–6]. The most appealing of their applications is a quantum computer in silicon[1,5,6], which has received much attention since its original proposal. Challenges concerning positioning and integration have hampered practical implementation so far. However, recent progress in dopant engineering[3,4,7], coherent control of dopant states[8–10], fault-tolerant design[5] and robust operation[11], together with proposals of entirely new schemes[12], provide fresh impetus to the development of devices based on the quantum functionality of single dopants.

One of the key elements of Si quantum electronics is control over the wavefunctions of dopants. This control is typically exercised by either a single or a combination of metallic gates. Being such a crucial point, a sizeable effort has been undertaken to understand the action of electric fields on dopants[13–22]. In the bulk limit, low fields lead to a small change in the eigenenergies of the donor[20,22], followed by ionization at higher fields[16,18]. In the other limit—a dopant close to the gate dielectric—it is possible to adiabatically pull the donor-bound electron into the potential well formed at the interface[19,23,24]. Here, we will focus on the latter case, as donors proximal to the interface provide an important mechanism for quantum functionality in a range of novel quantum device proposals. The hybridized donor–interface system, first investigated theoretically in ref 23, was recently proposed as the basis for quantum control of electron states at the interface[12].

The aggressive scaling of transistors in the semiconductor industry has led to devices where only about 100 dopants determine the device characteristics[25]. Such structures can provide electrical access to even smaller ensembles, down to the limit of a single dopant[26–28]. Here, we use state-of-the-art FinFETs to access single isolated As donors. The gate-induced shift of the single electron orbital states over a number of devices was measured. Fitting for the device parameters (donor depth and gate field strength) was carried out using an atomistic tight-binding device simulation. The device parameters thus determined were cross-checked against values determined from the measured charging energy and electrostatic modelling of the FinFETs.

We find that the theoretical description of all devices is in excellent agreement with the experimental data, thus providing a direct measure of the degree of hybridization of the electron wavefunction between the donor Coulomb well and the interfacial well. Across the devices measured, we find instances of the electron ground state confined in either the Coulomb well (full lattice symmetry) or in the interfacial well (reduced symmetry), as well as strong hybridization of higher orbital states. These measurements represent the first evidence of such a quantum-confinement transition as well as the ability to engineer the quantum state of a single donor electron by surface gate control.

The devices used in this study are three-dimensional field-effect transistors called FinFETs, which have their gate wrapped around three sides of the channel, see Fig. 1a. These FinFETs are a promising approach to address short-channel effects and leakage issues towards the 32 nm node[29]. The devices consist essentially of a p-type silicon nanowire connected to large source/drain electrodes. A second silicon nanowire, deposited perpendicular to the first and separated from it by a thin oxide, acts as a gate. The conventional

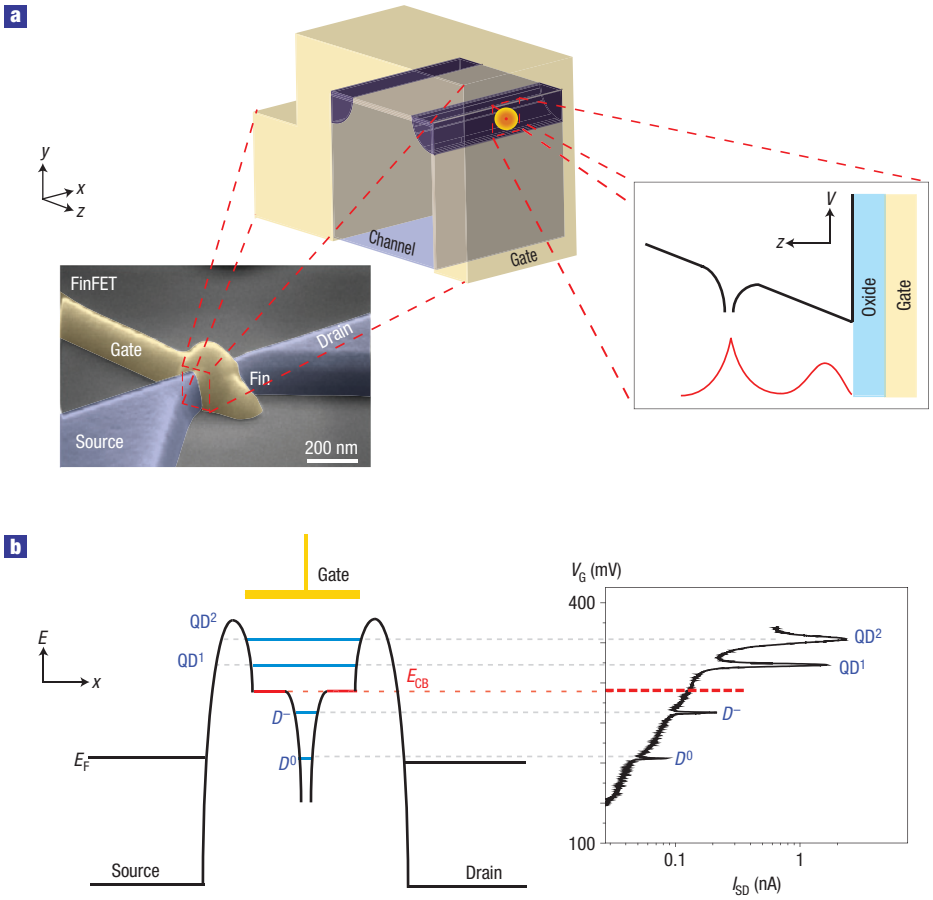

Figure 1 Geometry and electrical characteristics of a single donor located in the channel of a FinFET device. a, Coloured scanning electron micrograph of a typical FinFET device. Centre blow-up: Schematic diagram of the Si channel with the gate covering three of its faces. The channel and the wrap-around gate are separated by a nitrided oxide (1.4 nm equivalent SiO_2 thickness.) The corner regions are indicated in dark blue. The isolated donors studied here are necessarily located in these corner regions and are assumed to have diffused from the As source/drain contact extensions. Right blow-up: Band diagram along the *y* direction showing, from the right, the gate stack, the oxide, and the interface and Coulomb well with a wavefunction. **b**, Band diagram along the *x* direction with the D^0 state in resonance combined with the measured source/drain current versus gate voltage for a typical sample. QD^1 and QD^2 indicate resonances of a quantum dot, formed by the confinement provided by the corner effect and residual barriers in the access regions between the source/drain and the channel. The gate voltage where the band edge in the channel is aligned with the Fermi energy E_F in the source/drain, indicated by E_{CB}, is estimated by subtracting one unit of addition energy from QD^1. Below the band edge, there are resonances ascribed to the D^0 and D^- charge states of a single donor.

operation of this n–p–n field-effect transistor is to apply a positive gate voltage to create an inversion in the channel and allow a current to flow. Under our biasing condition, the current is not carried by the entire body of these FinFETs but only by its corners[30,31] (see Fig. 1a, centre blow-up). The cross-section of the current-carrying region is around 4 nm^2 (ref. 31).

From previous work, the active region of the FinFETs is known to be sufficiently small to be able to identify a single arsenic (As) donor in the channel[27]. Low-temperature conductance measurements show resonances due to the presence of the first and second electron states of the donor (the D^0 and D^- state, respectively) below the conduction band. The identification of these states was made on the basis of three criteria: the determined binding energies, the charging energy and the odd–even spin filling effect, which is discussed in detail in ref. 27. Applying these criteria to about 100 FinFETs with 60 nm gate length, we find six samples showing the typical pair of resonances of a single donor. Statistically, about one out of seven successfully measured samples shows the D^0 and D^- states. The others either do not show any resonances below the conduction band or show a complicated conductance spectrum probably due to (Coulomb) interactions between other nearby donors or defect states in the channel. We explain the frequent presence of donors in the p-type channel by transient enhanced diffusion at the $Si–SiO_2$ interface[32] originating from the As source/drain contact extensions.

Figure 1b shows a band diagram along the channel (*x* direction) combined with the measured source/drain current versus gate voltage for a sample showing a single donor. The gate voltage defines the chemical potential of the localized states and the current peaks whenever a state resides in the energy window of the bias voltage. The gate voltage at which a resonance occurs is thus a direct measure for the eigenenergy. The current maxima labelled QD^1 and QD^2 are resonances of a large quantum dot in the channel, formed by the confinement provided by the corner effect and residual barriers in the access regions between the source/drain and the channel[31]. The gate voltage at which the bottom of the conduction band in the channel is aligned with the Fermi energy, indicated by E_{CB}, is estimated by subtracting one unit of addition energy

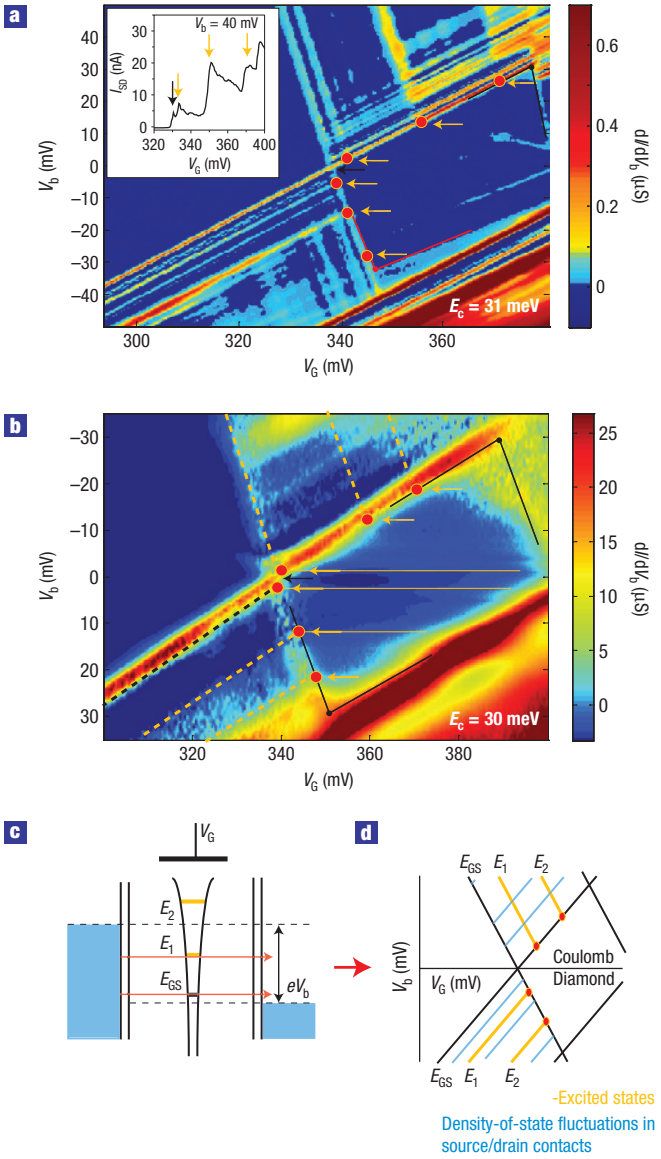

Figure 2 Excited-state spectroscopy data of single gated donors. **a**,**b**, Source/drain differential conductance of the D^0 charge state as a function of bias voltage and gate voltage in sample 13G14 (**a**) and sample 10G16 (**b**). Excited states are indicated by the red circles and yellow arrows. Accompanying inelastic cotunnelling lines within the Coulomb diamond are indicated by the thin solid lines. The inset in **a** shows source/drain current as a function of gate voltage at $V_b = 40$ mV. The black arrow indicates the ground state entering the bias window; the orange arrows indicate where the consecutive excited states enter. **c**, Schematic band diagram with the donor ground state (E_{GS}) and first excited state (E_1) in resonance. **d**, Schematic diagram showing the characteristic pattern for both excited states and density-of-states fluctuations in source/drain.

from the first quantum dot resonance. The donors, just like the large quantum dot, are located in the corner regions (with a lower potential than the rest of the channel) and are thus close to the Si–SiO_2 interface.

The focus of this article lies in the one-electron state (D^0) of a gated donor and its eigenenergies. The latter are determined from its stability diagram, that is, a plot of the differential conductance as a function of bias voltage and gate voltage, as shown for two devices in Fig. 2a,b, respectively. The D^0 state is separated from the D^- state by the Coulomb diamond-shaped region, where the current is Coulomb blockaded. The source/drain conductance inside the conduction regions depends on the number of donor levels available for transport (Fig. 2c), and peaks at each combination of bias and gate voltage where a new level enters the bias window (eV_b). This results in lines running parallel to the left-side edges of the diamond (and necessarily symmetric in V_b) in the stability diagram[33], indicated by the orange arrows and dashed lines. The pattern is schematically shown in Fig. 2d. The red dots indicate the bias voltage where excited states enter—and the ground state exits—the bias window, and are thus a direct measure for the excited-state energies ($eV_{b,N} = E_N$, where E_N is the Nth level relative to the ground state). We observe that visibility between excited states differs as it depends on the (relative) coupling of each excited state to the source and drain contacts. Excited states can furthermore be distinguished by clear steps in the source/drain current at the gate voltages where a new level enters the bias window, see Fig. 2a, inset. Samples with strong source/drain coupling show inelastic cotunnelling lines associated with some of the excited states inside the Coulomb diamond[34] (see Fig. 2c, horizontal orange lines), providing us with a further tool for the identification of levels. The conductance does not depend solely on the excited levels: we also observe a distinct pattern of parallel lines in the conducting regions due to density-of-state fluctuations in the source/drain contacts[35], compare again with Fig. 2c. As such, we have determined the first three excited states of six devices, as listed in the left column of Table 1. We estimate the experimental error on these values to be approximately 0.5 meV. The level spectra vary from sample to sample, but none of them resembles the spectrum of a donor in the bulk.

Table 1 First three measured excited states of each sample versus the best fit to a tight-binding (TB) model (NEMO 3D). The donor depths (under the Si–SiO_2 interface) that were obtained from the measured charging energy versus the distance obtained from the tight-binding fit are also given. The right-most column of the table lists the tight-binding predictions for the local electric field and the standard deviation of the fit *s*. The experimental error per level across all devices is approximately 0.5 meV.

Device		E_1 (meV)	E_2 (meV)	E_3 (meV)	E_C (meV)	d (nm)	F (MV m^{-1})	s (meV)
10G16	Exp.	2	15	23	30	3.3		
	TB	2.2	15.6	23.0		3.3	37.3	0.59
11G14	Exp.	4.5	13.5	25	29	3.2		
	TB	4.5	13.5	25.0		3.5	31.6	0.04
13G14	Exp.	3.5	15.5	26.4	31	3.5		
	TB	3.6	15.7	26.3		3.2	35.4	0.17
HSJ18	Exp.	5	10	21.5	33	4.0		
	TB	4.5	9.9	21.8		4.1	26.1	0.63
GLG14	Exp.	1.3	10	13.2	35	4.7		
	TB	1.3	10	12.4		5.2	23.1	0.28
GLJ17	Exp.	2	7.7	15.5	33	4.0		
	TB	1.3	7.7	15.8		4.9	21.9	0.77

The eigenenergies are a direct result of the electrostatic environment that confines the donor electron. The confinement potential in our system consists of the Coulomb potential of the donor nucleus and an induced triangular potential well at the Si–SiO_2 interface due to the gate electric field. This electric field is mainly generated by the mismatch in the electron affinity of the n-type polysilicon gate and the p-type channel[36]. We calculate the field throughout a device by solving the Poisson equation and the charge-distribution equation for our FinFETs self-consistently. In the corner regions where the donors are located, we find an electric

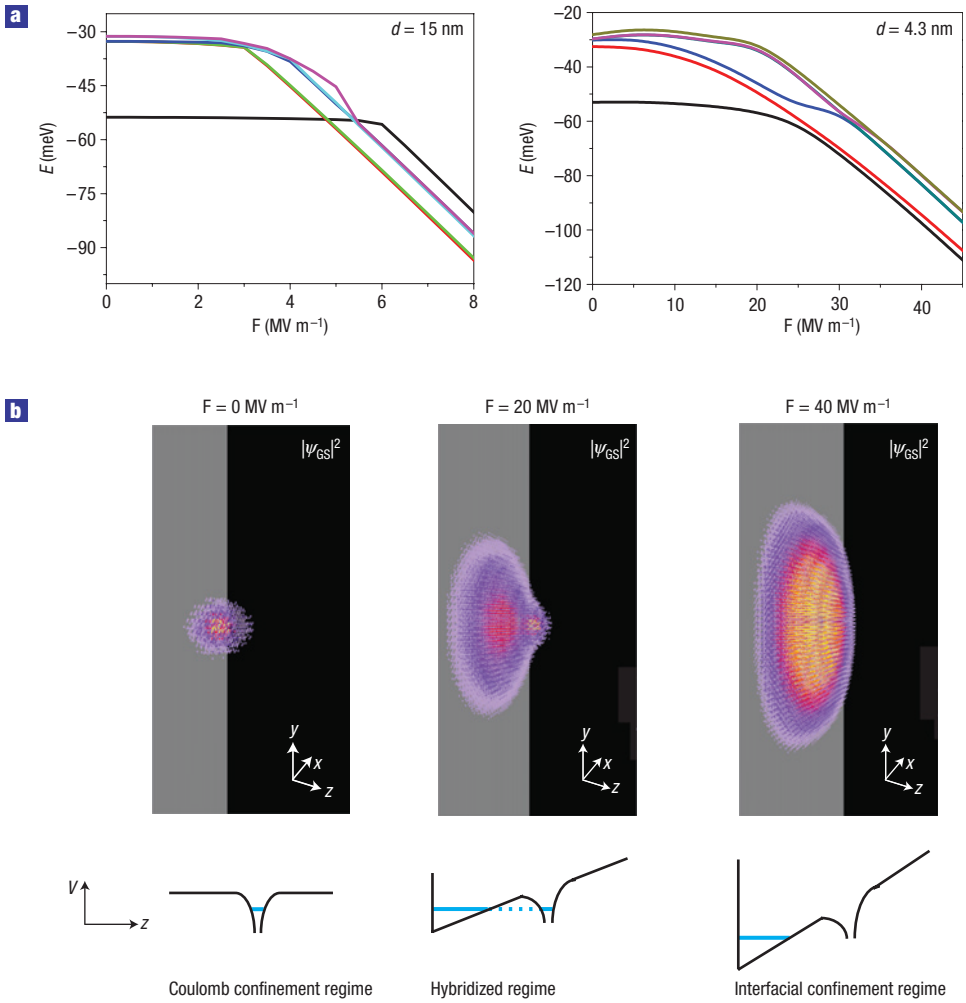

Figure 3 NEMO 3D (tight-binding) simulations of the gated donor eigenstates. a, First six eigenlevels of an As donor 15 nm (left) and 4.3 nm (right) below a SiO_2 interface as a function of electric field calculated in a tight-binding approximation (NEMO 3D). (Depicted eigenlevels might anticross with higher levels not shown in the graph.) **b**, Wavefunction density of the D^0 ground state ($|\psi_{GS}|^2$) for $d = 4.3$ nm in the three different electric field regimes: Coulomb confinement regime, 0 MV m^{-1} (left), hybridized regime, 20 MV m^{-1} (middle) and interfacial confinement regime, 40 MV m^{-1} (right). The grey plane indicates the Si–SiO_2 interface.

field (F) of around 21 MV m^{-1}. We know that the Coulomb field of the donor electron at a Bohr radius distance from the nucleus is around 30 MV m^{-1}. The gate field and the Coulomb field are thus comparable, which makes it clear that we do not expect a bulk-like As spectrum.

To calculate the eigenenergies of single gated donors in our FinFETs, we apply an atomistic tight-binding model implemented in NEMO 3D (Nanoelectronic Modeling tool, see refs 37,38). The tight-binding framework incorporating nanoelectronic gate fields was tested to high precision in the Stark shift of the donor hyperfine interaction against both experiment and momentum-space methods[22]. The levels of an As donor below a gate interface are numerically calculated as a function of local electric field F and donor depth d. Although the donor resides in a corner of the channel, the electrostatic environment determined from a self-consistent calculation is quite uniform with equipotential lines essentially following the curvature of the interface. Furthermore, as the typical curvature radius is twice that of the donor Bohr radius, we expect no significant confinement effects owing to the rounded edges. The planar geometry used in the theoretical model not only limits the number of variables in the problem, but turns out to give an excellent account of the essential physics of the gated donor system. The calculations include 1.4 million atoms corresponding to device volumes $30.4 \times 30.4 \times 30.4$ nm.

Figure 3 shows the first six eigenenergies versus electric field for $d = 15$ and 4.3 nm. The plotted energies are all relative to the conduction band at the donor site. Three separate confinement regimes are distinguished. Figure 3b shows the wavefunction density and schematic potential landscape for these three regimes at $d = 4.3$ nm. At low electric fields, the electron is located at the donor site and its ground state corresponds to a donor in bulk (thus, full lattice symmetry). At high electric fields, the electron is pulled inside the triangular potential well induced at the interface, reducing the symmetry of the system. The electron is still localized near the donor site in the lateral directions though, in correspondence with the results of refs 23,24. At the crossover between these regimes, the electron is delocalized over the donor and well sites. If the donor is 15 nm from the interface, the tunnelling rate between the two sites is low and no (significant) admixing of levels occurs. When the donor is close

to the interface, hybridization between 'donor-like' and 'well-like' states causes anticrossings with an energy gap of the order of several millielectronvolts, as can be readily observed from Fig. 3a. In these regions, the eigenstates of the system are being transformed to bonding- and antibonding-type states between the two sites. In contrast to interacting quantum dots[39] with their parabolic potential, the atomistic (Coulomb) potential of the donor nucleus is analogous to that of real molecules.

As both gate field (F) and donor depth (d) for each single donor device are unknown *a priori*, the measured levels are fitted by least-squares fits to the tight-binding prediction of the system over a range of F and d of 0–50 MV m^{-1} and 2.7–6.5 nm, respectively. The fit of the data to the tight-binding model is found to be quite good, as more elaborately discussed below. The fit furthermore yields the gate fields and donor depths for which the calculated level spectrum best matches the measured levels of each donor. The results are shown in Table 1. The predictions for d actually place our system in the important adiabatic regime of charge transfer from the donor site to the well site (at $d \sim 5$ nm).

The tight-binding model can also be used to identify and confirm the chemical nature of donors. The same fit to the data was also applied assuming phosphorus (P). The only relevant difference between the energy spectra of bulk As and P donors is the chemical splitting between the ground state and its higher excited states[40]. Taking into account the experimental error of 0.5 meV and assuming As donors, we obtain a reduced χ^2 across the six samples of 0.92, whereas for P donors we obtain 10.22. This clearly shows that the As model is the better estimator (two P fits are comparable in quality but not distinguishable within the error) and confirms the chemical nature of the donor as expected from the fabrication scheme.

The predictions made by the tight-binding model for the gate field (F) and donor depth (d) can be used to further confirm our atomistic understanding of these gated As donors in a nanostructure. We will compare these predictions with the electrostatics in the FinFET devices. First, the predicted d can be compared with a completely independent estimation made from the charging energy (E_C) between the As D^0 and D^- states. The charging energy follows from the stability diagram because the height of the Coulomb diamond, as also indicated in Fig. 2a,b, is a direct measure for this energy. We find the charging energy to be reduced compared with its bulk value (52 meV) and observe a clear trend for donors closer to the gate interface to have the largest reduction in charging energy, see Table 1. This is due to capacitive coupling to (mainly) the interface. A simple model (described in the Supplementary Information) using the geometric capacitances to quantitatively estimate d by the measured E_C yields a set of estimations that are close to—and follow the same trend as—the predictions of d obtained from the fit to the NEMO 3D model, see Table 1.

The predicted gate field and donor depth can be compared together with the electrostatic environment in the FinFET corner region. Figure 4 shows the positions of the donors in the field–donor depth plane as determined from the tight-binding fit (black data points). Most strikingly, there is a clear trend for donors closer to the interface to experience a larger electric field. As mentioned before, electrostatic modelling of the FinFETs yields a (device-independent) local electric of about 21 MV m^{-1}. The observed trend is attributed to the screening of the donor's dipole moment at the Si–SiO_2 interface (the same interface screening that is responsible for reducing the charging energy), which was not taken into account by the electrostatic FinFET modelling. Here, we make a quantitative approximation of the screening contribution to the local electric field by taking a classical approach. This basic model captures the observed magnitude and functional form of the

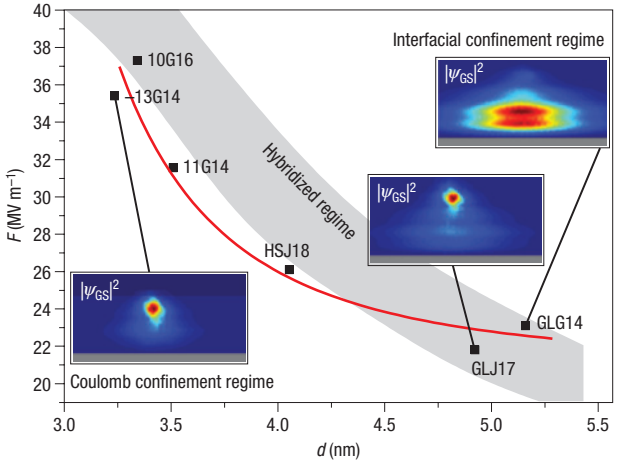

Figure 4 Local electric field F versus donor depth d of the As donors below the Si–SiO_2 interface as predicted by a fit to the tight-binding model, as also shown in Table 1. The red curve is a fit of the data to a classical model of interface screening as described in the Supplementary Information. The hybridized regime of the ground state is indicated by the grey band. Insets: Calculated ground-state wavefunctions of a few selected samples. The Si–SiO_2 interface is indicated in dark grey.

effect well, as shown in Fig. 4 by the red curve. We furthermore modelled the effect of the interface screening on the level spectrum at various relevant screening strengths and in refitting the data found only small changes in donor depth, in the range 0.1–0.4 nm, and local field changes less than a few per cent. The identification of quantum confinement across the six devices as shown in Fig. 4 was robust to this procedure. The fields and donor depths obtained from the NEMO 3D model are thus in good correspondence with the electrostatic environment in the FinFETs.

Depending on the combination of local field and donor depth, the electron is either confined by the Coulomb potential (3D symmetry) or the interface well (2D). In the transition from one extreme to the other, the ground state is a hybrid combination as indicated by the grey band in Fig. 4. The shape of the hybridized region was determined by analysing the ground-state wavefunctions and the anticrossing behaviour of the ground state with higher excited states in the energy versus local field plots of Fig. 3a. As can be readily observed, we find instances of the ground state being in all three regimes across the devices measured. The insets in Fig. 4 show the actual calculated wavefunctions for the devices in these particular regimes. Thus, the degree of hybridization of the ground state between the donor and the interface can be determined from the experimental level spectrum in tandem with the theoretical model. The theoretical analysis further shows how this is tunable as a function of the gate-induced electric field and the donor depth.

Together with the atomistic understanding of the donor environment, the tight-binding model offers a precise description of a real gated donor in a nanostructure, accurate enough to clearly identify the chemical nature of the donors involved. Furthermore, we understand the effects—from donor/well hybridization and symmetry change to interface screening—that play a major role in the description of these systems. Together with the recent progress in dopant engineering, the physical understanding of (experimentally realized) gated donors makes the development of complex logical structures using donors states in silicon viable. Control over the hybridization and symmetry in donor–quantum

well or donor–donor systems incorporated in a semiconductor host could for instance be used to create molecular-type systems in the solid state. Such structures facilitate logic beyond a simple switch in a similar manner as has been shown for organic molecules[41,42], without the inherent disadvantages resulting from chemical instability and contacting issues.

METHODS

The FinFET devices consist of a narrow crystalline silicon wire (fin) acting as a channel with large contacts patterned by 193 nm optical lithography and dry etching in a 60 nm layer of silicon-on-insulator. After a boron channel implantation, 100 nm of polycrystalline silicon was deposited on top of a nitrided oxide (1.4 nm equivalent SiO_2 thickness), then received a phosphorus (P) implant as predoping, and was patterned using an oxide hard mask to form a narrow gate. The polycrystalline gate wire was deposited perpendicularly to the channel wire and forms a gate on three of its faces. Next, we used high-angle As implantations as source or drain extensions, while the channel was protected by the gate and 50-nm-wide nitride spacers and remained p-type. Finally, As and P implants and a NiSi metallic silicide were used to complete the source or drain electrodes.

The conventional operation of this n–p–n field-effect transistor is to apply a positive gate voltage to create an inversion in the channel and allow a current to flow. However, the corner regions of the channel nanowire (indicated in dark blue in Fig. 1a) go into inversion at a lower applied potential than the rest of the channel. This effect is well established for these wrap-around gate transistors and is known as the corner effect. It originates from the increased capacitive coupling of these corner regions to the gate, which decreases the potential in the corners compared with the rest of the channel[43]. Any As donors present in these corner regions are necessarily close to the Si–SiO_2 interface separating the Si channel nanowire and the wrap-around gate.

The Bohr field F_{donor} due to the long-range Coulomb potential of the donor is nearly equal to (and can thus be estimated by) the field of a single positive charge located at the As site; thus, $F_{\mathrm{donor}} = (e/4\pi\epsilon r^2)$, where e is the unit charge, ϵ is the dielectric constant of Si and r is the distance to the nucleus.

In the least-squares fit of a sample to the tight-binding model, we fit three excited states to a model with two degrees of freedom, namely F and d. The standard deviation of the fit should in this case be interpreted as the error between the data and the model for each sample. This model-based error is a result of, among other things, the planar approximation and the no-screening approximation discussed below. The measurement error on the identified levels across all devices is around 0.5 meV, and is mainly due to the lifetime broadening of the excited states.

All of the measurements are carried out in a pumped helium-4 system at 1.6 K.

Received 22 November 2007; accepted 9 May 2008; published 15 June 2008.

References

1. Kane, B. E. A silicon-based nuclear spin quantum computer. *Nature* **393**, 133–137 (1998).
2. Vrijen, R. *et al.* Electron-spin-resonance transistors for quantum computing in silicon–germanium heterostructures. *Phys. Rev. A* **62**, 012306 (2000).
3. Ruess, F. *et al.* Realization of atomically controlled dopant devices in silicon. *Small* **3**, 563–567 (2007).
4. Jamieson, D. N. *et al.* Controlled shallow single-ion implantation in silicon using an active substrate for sub-20-keV ions. *Appl. Phys. Lett.* **86**, 202101 (2005).
5. Hollenberg, L. C. L. *et al.* Charge-based quantum computing using single donors in semiconductors. *Phys. Rev. B* **69**, 113301 (2004).
6. Hollenberg, L. C. L., Greentree, A. D., Fowler, A. G. & Wellard, C. J. Two-dimensional architectures for donor-based quantum computing. *Phys. Rev. B* **74**, 045311 (2006).
7. Shinada, T., Okamoto, S., Kobayashi, T. & Ohdomari, I. Enhancing semiconductor device performance using ordered dopant arrays. *Nature* **437**, 1128–1131 (2005).
8. Huebl, H. *et al.* Phosphorus donors in highly strained silicon. *Phys. Rev. Lett.* **97**, 166402 (2006).
9. Andresen, S. E. S. *et al.* Charge state control and relaxation in an atomically doped silicon device. *Nano Lett.* **7**, 2000–2003 (2007).
10. Stegner, A. R. *et al.* Electrical detection of coherent ^{31}P spin quantum states. *Nature Phys.* **2**, 835–838 (2006).
11. Testolin, M. J., Hill, C. D., Wellard, C. J. & Hollenberg, L. C. L. Robust controlled-NOT gate in the presence of large fabrication-induced variations of the exchange interaction strength. *Phys. Rev. A.* **76**, 012302 (2007).
12. Calderòn, M. J., Koiller, B., Hu, X. & Das Sarma, S. Quantum control of donor electrons at the Si/SiO_2 interface. *Phys. Rev. Lett.* **96**, 096802 (2006).
13. Larionov, A. A., Fedechkin, L. E., Kokin, A. A. & Valiev, K. A. The nuclear magnetic resonance spectrum of ^{31}P donors in a silicon quantum computer. *Nanotechnology* **11**, 392–396 (2000).
14. Wellard, C. J., Hollenberg, L. C. L. & Pakes, C. I. Single-qubit operations on the Kane quantum computer. *Nanotechnology* **13**, 570–575 (2002).
15. Kettle, L. M. *et al.* Numerical study of hydrogenic effective mass theory for an impurity P donor in Si in the presence of an electric field and interfaces. *Phys. Rev. B* **68**, 75317 (2003).
16. Smit, G. D. J., Rogge, S., Caro, J. & Klapwijk, T. M. Stark effect in shallow impurities in Si. *Phys. Rev. B* **70**, 035206 (2004).
17. Wellard, C. J. & Hollenberg, L. C. L. Donor electron wavefunctions for phosphorus in silicon: Beyond effective-mass theory. *Phys. Rev. B* **72**, 085202 (2005).
18. Friessen, M. Theory of the Stark effect for P donors in Si. *Phys. Rev. Lett.* **94**, 186403 (2005).
19. Debernardi, A., Baldereschi, A. & Fanciulli, A. Computation of the Stark effect in P impurity states in silicon. *Phys. Rev. B* **74**, 035202 (2006).
20. Bradbury, F. R. *et al.* Stark tuning of donor electron spins in silicon. *Phys. Rev. Lett.* **97**, 176404 (2006).
21. Hui, H. T. Numerical method for determination of the NMR frequency of the single-qubit operation in a silicon-based solid-state quantum computer. *Phys. Rev. B* **74**, 195309 (2006).
22. Rahman, R. *et al.* High precision quantum control of single donor spins in silicon. *Phys. Rev. Lett.* **99**, 036403 (2007).
23. Martins, A. S., Capaz, R. B. & Koiller, B. Electric-field control and adiabatic evolution of shallow donor impurities in silicon. *Phys. Rev. B* **69**, 085320 (2004).
24. Calderòn, M. J., Koiller, B. & Das Sarma, S. External field control of donor electron exchange at the Si/SiO_2 interface. *Phys. Rev. B* **75**, 125311 (2007).
25. Asenov, A. Random dopant induced threshold voltage lowering and fluctuations in sub 50 nm MOSFETs: A statistical 3D 'atomistic' simulation study. *Nanotechnology* **10**, 153–158 (1999).
26. Calvet, L. E., Wheeler, R. G. & Reed, M. A. Observation of the linear Stark effect in a single acceptor in Si. *Phys. Rev. Lett.* **98**, 096805 (2007).
27. Sellier, H. *et al.* Transport spectroscopy of a single dopant in a gated silicon nanowire. *Phys. Rev. Lett.* **97**, 206805 (2006).
28. Hofheinz, M. *et al.* Individual charge traps in silicon nanowires. *Eur. Phys. J. B* **54**, 299307 (2006).
29. Rooyackers, R. *et al. Doubling or Quadrupling MuGFET Fin Integration Scheme with Higher Pattern Fidelity, Lower CD Variation and Higher Layout Efficiency* 993–996 (IEDM Tech. Dig., 2006).
30. Neophytou, N., Paul, A., Lundstrom, M. S. & Klimeck, G. *Proc. 12th Int. Conf. on Simulation of Semiconductor Devices and Processes (SISPAD), Vienna Austria, September 25–27* (2007).
31. Sellier, H. *et al.* Subthreshold channels at the edges of nanoscale triple-gate silicon transistors. *Appl. Phys. Lett.* **90**, 073502 (2007).
32. Kasnavi, R. *et al.* Characterization of arsenic dose loss at the Si/SiO_2 interface. *J. Appl. Phys.* **87**, 2255 (2000).
33. Kouwenhoven, L. P. *et al.* in *Mesoscopic Electron Transport* (eds Sohn, L. L., Kouwenhoven, L. P. & Schn, G.) (Kluwer, Dordrecht, 1997).
34. Schleser, R. *et al.* Cotunneling-mediated transport through excited states in the Coulomb-blockade regime. *Phys. Rev. Lett.* **94**, 206805 (2005).
35. Björk, M. T. *et al.* Few-electron quantum dots in nanowires. *Nano Lett.* **4**, 1621–1625 (2004).
36. Sze, S. *Physics of Semiconductor Devices* 2nd edn 397 (Wiley, New York, 1981).
37. Klimeck, G., Oyafuso, F., Boykin, T. B., Bowen, R. C. & von Allmen, P. Development of a nanoelectronic 3D (NEMO 3D) simulator for multimillion atom simulations and its application to alloyed quantum dots. *Comput. Modeling Eng. Sci.* **3**, 601–642 (2002).
38. Klimeck, G. *et al.* Atomistic simulation of realistically sized nanodevices using NEMO 3D: Part I—models and benchmarks. *IEEE Trans. Electron Dev.* **54**, 2079–2089 (2007).
39. Bayer, M. *et al.* Coupling and entangling of quantum states in quantum dot molecules. *Science* **291**, 451–453 (2001).
40. Ramdas, A. K. & Rodriguez, S. Spectroscopy of the solid-state analogues of the hydrogen atom: Donors and acceptors in semiconductors. *Rep. Prog. Phys.* **44**, 1297–1387 (1981).
41. Joachim, C., Gimzewski, J. K. & Aviram, A. Electronics using hybrid-molecular and mono-molecular devices. *Nature* **408**, 541–548 (2000).
42. Vandersypen, L. M. K. *et al.* Experimental realization of Shor's quantum factoring algorithm using nuclear magnetic resonance. *Nature* **414**, 883–887 (2001).
43. Xiong, W., Park, J. W. & Colinge, J. P. Corner effect in multiple-gate SOI MOSFETs, *SOI Conf., 2003. IEEE Int.*, 111–113 (2003).

Supplementary Information accompanies this paper on www.nature.com/naturephysics.

Acknowledgements

This project is supported by the Dutch Foundation for Fundamental Research on Matter (FOM), the Australian Research Council, the Australian Government, the U.S. National Security Agency (NSA) and the Army Research Office (ARO) under Contract No. W911NF-04-1-0290. Part of this work was done at JPL, Caltech under a contract with NASA. NCN/nanohub.org computational resources were used. We thank P. E. Rutten and D. S. Ebert for their contribution.

Author contributions

Experiments were carried out at Delft University of Technology (G.P.L., J.C., S.R.) with devices fabricated by IMEC (N.C., S.B.); modelling was done at University of Melbourne (C.J.W., L.C.L.H.) and Purdue University (R.R., I.W., G.K.).

Author information

Reprints and permission information is available online at http://npg.nature.com/reprintsandpermissions. Correspondence and requests for materials should be addressed to G.P.L.